Non-Invasive Imaging of Cellulose Microfibril Orientation within Plant Cell Walls by Polarized Raman Microspectroscopy

Lan Sun[1ab,2], *Seema Singh*[1b,2], *Michael Joo*[3b], *Miguel Vega-Sanchez*[1c,3a,#], *Pamela Ronald*[1c,4], *Blake A. Simmons*[1b,2], *Paul Adams*[1a,3a,5], *Manfred Auer*[1a,3b*]

[1a]Technology Division, [1b]Deconstruction Division, [1c]Feedstocks Division, Joint BioEnergy Institute, Lawrence Berkeley Laboratory, 5885 Hollis Street, Emeryville, CA94608

[2]Biological and Engineering Sciences Center, Sandia National laboratories, P.O. Box 969, Livermore, CA 94551

[3a]Physical Biosciences Division, [3b]Life Sciences Division, Lawrence Berkeley Laboratory, One Cyclotron Road, Berkeley, CA 94720

[4]Department of Plant Pathology and the Genome Center, University of California, Davis, One Shields Ave., Davis, CA 95616

[5]Department of Bioengineering, University of California, Berkeley, 306 Stanley Hall, Berkeley, CA 94720

*Corresponding Author: Manfred Auer
Address: Life Sciences Division, Lawrence Berkeley Laboratory, One Cyclotron Road, Berkeley, CA 94720; Phone: 510-486-7702; Fax: 510-486-6488; Email: mauer@lbl.gov

#Current affiliation: Monsanto Company, Chesterfield Village, Chesterfield, MO 63017

Running Title: Raman imaging of Cellulose Microfibril Orientation

ABSTRACT

Cellulose microfibrils represent the major scaffold of plant cell walls. Different packing and orientation of the microfibrils at the microscopic scale determines the macroscopic properties of cell walls and thus affect their functions with a profound effect on plant survival. We developed a polarized Raman microspectroscopic method to determine cellulose microfibril orientation within rice plant cell walls. Employing an array of point measurements as well as area imaging and subsequent Matlab-assisted data processing, we were able to characterize the distribution of cellulose microfibril orientation in terms of director angle and anisotropy magnitude. Using this approach we detected differences between wild type rice plants and the rice *brittle culm* mutant, which shows a more disordered cellulose microfibril arrangement, and differences between different tissues of a wild type rice plant. This novel non-invasive Raman imaging approach allows for quantitative assessment of cellulose fiber orientation in cell walls of herbaceous plants, an important advancement in cell wall characterization.

KEYWORDS: Cellulose microfibril orientation, polarized Raman microspectroscopy, plant cell wall, *brittle culm* mutant, director angle, anisotropy magnitude

INTRODUCTION

Cellulose microfibrils represent the major scaffold of plant cell walls. Multiple strands of repeating β-1-4 linking cellobiose units are closely arranged into a filamentous structure, also known as cellulose microfibrils. Their packing into ordered arrays and supramolecular organization at the microscopic scale determines the macroscopic mechanical properties of cell walls and thus affects their functions with a profound effect on plant survival (Booker and Sell 1998), and with high significance for many industrial applications (Goswami et al. 1996; Madakadze et al. 1999; Varanasi et al. 2012). Due to this importance of cellulose microfibril orientation for cell wall properties, non-invasive measurement techniques that allow determination of microfibril organization are highly desirable by plant biologists and industrial users of plant materials in order to better understand and control the physical properties of these materials.

Cellulose microfibril orientation is often described by the term microfibril angle (MFA) in wood science, referring to the angle between the direction of the helical windings of cellulose microfibrils in the secondary cell wall of fibers and tracheids and the long axis of the cell. A review article by Donaldson (2008) presents a comprehensive summary of techniques to measure MFA and divides them into two categories, either measurement of individual tracheids or fibers using microscopy or measurement of bulk wood samples using X-ray diffraction or near infrared (NIR) spectroscopy. Polarization microscopy (Palviainen et al. 2004; Ye 2006), differential interference contrast (DIC) microscopy (Peter et al. 2003), scanning electron microscopy (Abe et al. 1991), and transmission electron microscopy (Donaldson and Xu 2005) are some representative microscopic techniques for MFA measurement. Furthermore biological, chemical

or physical treatments of wood samples have been adopted by some researchers to help visualize the orientation of the microfibrils, such as iodine staining (Donaldson and Frankland 2005) and ultrasonic treatment (Huang 1995). X-ray diffraction is currently perhaps the most popular method for measuring MFA, and given its simplicity can be applied to a single wall or to strips of wood several millimeters in thickness, and thus is very convenient for determining average MFA (Barnett and Bonham 2004; Cave 1997). NIR spectroscopy can be used to estimate MFA among a range of other wood properties for a large number of wood samples based on calibrations established by the measured physical properties (Schimleck et al. 2001a; Schimleck et al. 2001b). MFA predicted by NIR was found to be in excellent agreement with MFA determined by X-ray diffractometry (Schimleck and Evans 2002).

Although these measurement techniques have been used to measure MFA of individual fibers or bulk wood samples, limited work has been done to investigate the distribution of cellulose microfibril orientation within cell walls. Position-resolved property determination is important for a variety of applications, as the distribution of MFA within different layers of cell walls, cell walls of different tissues, and cell walls from different parts of a plant may vary significantly, resulting in differences in overall wood properties (Barnett and Bonham 2004). For example, for biofuel production, researchers are engineering lignocellulosic feedstocks for easier deconstruction. However, the effect on mechanical strength of the plant cannot be easily predicted. Therefore, the distribution of MFA within cell walls and across different cell types can be used to evaluate and predict mechanical strength of these mutant plants, which will ultimately allow researchers to make predictions for their survival in the wild/field. However, in order to acquire this position-resolved information, microscopic imaging with sufficient spatial resolution

is required. Attempts have been made to study the helical arrangement of cellulose fibrils in the S2 layer of adjacent wood cells using synchrotron X-ray imaging (Lichtenegger et al. 1999). However, this tool is often not easily accessible due to the limited number of facilities that have a synchrotron light source. In addition, the X-ray beam size of 2 μm is not small enough to provide high-resolution imaging within individual cell walls. Infrared imaging, another promising approach for studying cell wall organization, can be used to acquire position-resolved chemical compositions of plant cell walls (Dokken et al. 2005). However, due to the low sensitivity caused by non-background-free detection, the low spatial resolution associated with the long infrared wavelengths, and water absorption of the infrared light, this technique is somewhat limited (Evans and Xie 2008).

In contrast to the limitations posed by these approaches, Raman microspectroscopy offers several attractive advantages. First, nondestructive measurements with strong chemical selectivity and specificity towards major cell wall components can be performed with minimum sample preparation and without any interference from water. Second, submicron spatial resolutions can be achieved to provide tissue and cell type specific compositional information about cell walls (Agarwal 2006; Gierlinger and Schwanninger 2006; Sun et al. 2013; Sun et al. 2011). Third, by controlling the polarization direction of the incoming excitation laser, orientation information about the cell wall components can be acquired. Therefore, due to the chemical selectivity and specificity of this technique, this approach has the potential to monitor both the structural and chemical changes of the cell walls, including plant biomass that was chemically or genetically modified. In addition, unlike the limited access to a synchrotron light

source, commercial and home built Raman microspectroscopy instruments are available to a broad scientific community.

Point measurement of macromolecular orientation in fibers and plant cell walls by polarized Raman spectroscopy was demonstrated in earlier studies (Agarwal and Atalla 1986; Atalla and Agarwal 1985; Atalla et al. 1980; Cao et al. 2006; Kovur et al. 2008). In a more recent study, Gierlinger et al. (2010) established a partial least square (PLS) regression model between the spectral intensity ratio and the angle of laser polarization for black spruce to predict MFA distribution based on spectra extracted from Raman images of black spruce cell walls. However, this approach relied on a PLS model that was developed based on a single fiber, and the Raman images were only collected with two incident laser polarization directions perpendicular to each other. To obtain accurate prediction of the MFA distribution in cell walls, a perfect perpendicular alignment between the fiber axis and the cross-sectional area for the model fiber and a perfect parallel alignment between the radial or tangential cell walls with the laser polarization direction were required, which was difficult to accomplish in that study. Also, the differences between the model fiber and the cell wall specimen may cause inaccurate prediction of MFA in the cell wall, since the polarization-angle-dependent Raman profile can vary from pixel to pixel.

In this work, we performed polarized Raman microspectroscopy to study the spatial distribution of cellulose microfibril orientation in rice cell walls. Instead of using just two laser polarization directions, we performed a complete polarization-resolved procedure by collecting 36 Raman images at 10° intervals around the excitation polarization direction. This approach is not impacted by heterogeneity of the angle-resolved Raman profile from pixel to pixel caused by heterogeneity of cell wall compositions at different positions, since the angle-resolved Raman

profile is generated at every pixel independently and calculation is not relying on calibration models obtained using calibration samples different from the specimen of interest. Thus, this approach can be used to determine cellulose microfibril orientation at different positions in cell walls more accurately. In addition, we overcame the significant challenge of data processing for complete polarization-resolved Raman imaging by developing Matlab codes to process a large number of data sets simultaneously (Matlab code is available upon request). Through this technique, we observed clear differences in cellulose microfibril orientation between different tissues of the wild type rice plant as well as between the wild type and the *brittle culm* mutant, a mutant compromised in secondary cell wall deposition.

MATERIALS AND METHODS

Materials and Sample Preparation

Wild type rice and *brittle culm* (*bc*) rice mutant were used for this study. The mutant (RGT3584-bc) and wild type control (a segregant line not containing the transposon insertion: RGT3584-WT) are in the cultivar Nipponbare background and were obtained from the Rice Insertional Mutation Database, Sundaresan Lab at UC Davis. The RGT3584-bc mutant contains an Ac/Ds transposon insertion in the locus of the rice *OsCesA7* gene, which encodes for a subunit of the Cellulose Synthase (CESA) complex involved in the biosynthesis of cellulose in secondary cell walls of rice (Tanaka et al. 2003). We have previously shown that this mutant contains both reduced cellulose content (Smith-Moritz et al. 2011) and severely compromised mechanical strength (Varanasi et al. 2012). Plants were grown in growth chambers as described in Vega-Sanchez et al. (2012), and samples were collected at the full senescence stage.

The senesced, dry leaf sheath sections were hand cut into small pieces and directly used for point measurement. For Raman imaging, dry plant samples were embedded in LR white resin using a protocol similar to transmission electron microscopy, except that samples did not undergo any fixation or heavy metal staining. Samples were dehydrated at room temperature in a graded aqueous ethanol series (25%, 50%, 75%, v/v, 3 min for each step) followed by three incubations (5 min each) in 100% ethanol. Samples were infiltrated with LR White resin in a graded LR White/ethanol series (25%, 50%, 75% v/v, 3 min for each step) followed by three incubations (5 min each) in 100 % resin. After polymerization at 65˚C for 2 days, a LR White embedded sample was first cut in half longitudinally so that the closed, hollow cylindrical shape became an open U-shaped structure, which was then sectioned longitudinally with an ultramicrotome (Leica, Buffalo Grove, IL). The sections from the ultramicrotome were thin rectangles at a nominal thickness of 500 nm or 1 µm. These sections were transferred to glass slides for Raman imaging.

Polarized Raman Microspectroscopy

All the measurements were performed using a LabRam HR 800 confocal Raman system equipped with a 785 nm laser (Horiba Jobin Yvon, Edison, NJ). A high numerical aperture 100× (oil NA 1.40) objective was used to acquire all the spectra. For point measurement of the leaf sheath sections, integration time was 20 s for the wild type plant and 80 s for the *brittle culm* mutant, respectively. For imaging, a marked area of 2.5 µm by 3.0 µm was scanned at a mapping step of 0.5 µm with an integration time of 3 s for the leaf sheath section. A marked area of 1.0 µm by 3.0 µm was scanned at a mapping step of 0.5 µm with an integration time of 5 s for the stem and leaf sections. The estimated laser spot size was ~0.7 µm. The laser penetration depth

was very sample dependent and the maximum penetration would probably be about 5 to 10 μm. The raster mapping technique was utilized in SWIFT mode (the stage triggers the detector at specific positions and acquisition is done “on the fly”) to significantly increase mapping speed. The grating was 300 g/mm and the spectral resolution was ~11 cm^{-1}. The polarization direction of the excitation laser was changed in increments of 10° by rotating the half-wave plate manually. Both point measurements and Raman imaging were performed at every polarization direction ranging from 0° to 360° at an interval of 10°.

Data Processing

The raw Raman spectra in the range of interest were pre-processed using the LabSpec5 software (Horiba Jobin Yvon, Edison, NJ), which sequentially removes spikes, corrects baselines, smoothes the spectra by the Savitsky-Golay algorithm at a moderate level, and then further smoothes the data by Fourier transformation coupled with cosine apodization function. A Matlab code (the code is available upon request) was developed to determine intensity at the characteristic peak of interest and perform ellipse fitting to determine the two parameters that define the fiber orientation, director angle and anisotropy magnitude, for all measurement positions. Here, for each position (x, y) in the plant section for measurement, the maximum intensity as a function of excitation polarization is denoted by $I_{max}(x, y)$, and the orientation of the excitation polarization associated with this intensity is indicated by $\phi_{max}(x, y)$, the director angle. The minimum intensity as a function of excitation polarization is denoted by $I_{min}(x,y)$. $I_{max}(x, y)$ and $I_{min}(x,y)$ can be determined by ellipse fitting of the intensity data as a function of excitation

9

polarization. Thus, the anisotropy magnitude, ρ(x, y), can be calculated by Equation 1 (Zimmerley et al. 2010)

$$\rho(x,y)=\frac{I_{max(x,y)}-I_{min(x,y)}}{I_{max(x,y)}+I_{min(x,y)}} \quad (1)$$

RESULTS AND DISCUSSION

We utilized the orientation dependency of the characteristic Raman peak of cellulose in order to determine the cellulose microfibril orientation. The experimental set-up is shown in Figure 1. The polarization direction of the excitation laser was controlled by a half-wave plate. When the half-wave plate is rotated 1 θ degree, polarization of the incident laser is rotated 2 θ degree. In this study, the rotation step (θ) was 5 degrees and data was therefore collected every 10 degrees. In principle, when the cellulose microfibril orientation is parallel to the polarization direction of the excitation laser, the maximum Raman intensity of the characteristic cellulose peak will be obtained. When the cellulose microfibril orientation is perpendicular to the polarization direction of the excitation laser, the minimum Raman intensity of the same peak will be obtained. Thus, by ellipse fitting of the intensity data as a function of excitation polarization, we determined the maximum and minimum Raman intensity of the characteristic cellulose peak and hence the cellulose microfibril orientation.

To demonstrate the concept of detection, we used a longitudinal leaf sheath section of wild type (RGT3584-WT, cv. Nipponbare) rice as a model system. Raman spectra in the range of 200-1700 cm^{-1} as a function of polarization direction of the excitation laser are shown in Figure 2a. It can be clearly seen in the zoomed-in spectral range of 1017-1218 cm^{-1} (see Figure 2b) that the intensity of the two major cellulose peaks, 1095 cm^{-1} and 1122 cm^{-1}, assigned to backbone

stretching (Wiley and Atalla 1987), was changing with the change of polarization direction of the excitation laser. We observed a more significant change at 1095 cm^{-1}, as confirmed by ellipse fitting of the peak intensity as a function of the polarization direction of the excitation laser for both cellulose peaks (see Figure 2c, d). $I_{max}(x, y)$ and $I_{min}(x, y)$ are the long and short axes of the fitted ellipses, respectively, and the anisotropy magnitudes can then be calculated accordingly as the ratio of the differences between $I_{max}(x, y)$ and $I_{min}(x, y)$ over the sum of $I_{max}(x, y)$ and $I_{min}(x, y)$. The anisotropy magnitude of the peak at 1095 cm^{-1} ($\rho = 0.21$) is significantly higher than that of the peak at 1122 cm^{-1} ($\rho = 0.09$), indicating that the peak at 1095 cm^{-1} has a stronger dependence on excitation polarization. Thus, this peak was used in this study to determine cellulose microfibril orientation, and for this particular cell wall position, the director angle in wild type was found to be 30° (see Figure 2c). In addition to the cellulose peak, we also tested the dependence on excitation polarization of the lignin peak at 1600 cm^{-1}, assigned to symmetric stretching of the aromatic ring (Atalla and Agarwal 1985; Atalla and Agarwal 1986). As shown in Figure 2e, we did not observe a significant dependence of Raman intensity at 1600 cm^{-1} as a function of changes in the direction of excitation polarization, indicating that there is no preferred orientation of aromatic rings of lignin in the longitudinal plane of the leaf sheath section of the wild type rice plant. Our result for lignin is similar to previous observations in the latewood fiber of spruce (*Picea abies*) (Gierlinger et al. 2010), but is different from previous results obtained from the secondary wall in early wood tissue of black spruce (*Picea mariana*) (Atalla and Agarwal 1985). It should be noted that there was negligible contribution of signal from LR white for the spectral ranges of interest in this work. Since we were using low grating

(300 g/mm) in this work, the differences in grating's reflectivity at different polarization direction were negligible.

Using the method described above, we conducted the first study, to our knowledge, that uses polarized Raman microspectroscopy to detect differences of cellulose microfibril orientation in cell walls between wild type and mutant herbaceous plants. We focused on leaf sheath sections of wild type and *brittle culm* rice plants as our model samples. Grass *brittle culm* mutants display compromised mechanical strength properties in diverse plant tissues and are associated with defects in cellulose biosynthesis and/or deposition in the plant cell wall (Zhang and Zhou 2011). Field emission scanning electron microscopy had previously been used to examine the innermost secondary walls of wild type and *brittle culm 12* (*bc12*) rice plants and showed that wild-type fibers were packed in a parallel pattern, whereas those of the mutant plants were arranged in a random manner. Combined with additional compositional analysis of cell walls, the study concluded that the inferior mechanical strength of *bc12* is probably caused by the altered wall composition and aberrantly deposited cellulose microfibrils in the secondary walls (Zhang et al. 2010). However, previous work characterizing herbaceous plant mutants had to measure composition and packing pattern of the cellulose microfibrils separately and hence was not able to obtain these two pieces of information from the same section of a sample. Also, previous work was not able to provide quantitative information about cellulose microfibril orientation. Our proposed method, on the other hand, can directly and quantitatively reveal the differences between wild type and mutant plants in both compositional information and microfibril orientation at the specified location within the plant cell walls.

As shown in Figure 3, we observed differences in microfibril orientation when comparing leaf sheath samples between wild type and *bc* rice plants using point measurements. We marked six points in a single cell wall of the wild type and mutant samples in the bright field images (see Figure 3a, c) for polarized Raman measurements (see Figure 3b, d). By plotting the Raman intensity at 1095 cm^{-1} as a function of polarization direction of the excitation laser and ellipse fitting, we determined the director angle and thus the cellulose microfibril orientation at specific positions within the cell wall (see Figure 3b, d). For the wild type sample, we determined the director angle as 20° between the cellulose microfibrils and the longitudinal axis of the cell wall. The director angle was relatively constant for each of the measured points in the cell wall, indicating an ordered overall arrangement of the cellulose microfibrils. In contrast, we did not observe any constant director angle for the positions within the cell wall of the *brittle culm* mutant sample, indicating a more random arrangement of the cellulose microfibrils. The distinct differences in the cellulose microfibril orientation between the wild type and mutant plants were also evident from significant difference in the anisotropy magnitude (see Figure 3b, d). The *brittle culm* mutant was determined previously to have compromised mechanical strength (Varanasi et al. 2012), indicating that cellulose microfibril orientation in cell walls might be related with mechanical strength of plants. It should be noted that while an integration time of 20 s was used for the wild type plant, due to low cellulose signal we used a significantly longer integration time (80 s) for the mutant plant. This indicates that cellulose content was significantly reduced in the mutant, which is consistent with previous observation (Smith-Moritz et al. 2011; Tanaka et al. 2003).

Using a similar concept as demonstrated above, we were able to reveal the spatial distribution of cellulose microfibril orientation within plant cell walls in terms of director angle, $\phi_{max}(x, y)$, as well as anisotropy magnitude, $\rho(x, y)$, by Raman microspectroscopy or Raman imaging that has the advantages of high spatial resolution and chemical specificity. Essentially, we first chose the area of interest within the cell wall and generated grids for imaging. Then we scanned the marked area by collecting Raman spectra from each position on the mapping grids. We repeated the same procedure at every polarization direction of the excitation laser and thus generated 36 Raman maps. It took less than 2 h to collect all of these 36 maps with our setting. We didn't observe much drift (< 0.5 μm, the mapping step) over time for the thin and flat section for imaging, and thus our data acquisition/processing method does not account for drift. This polarization-resolved imaging approach is not limited by heterogeneity of the polarization profile from pixel to pixel and can determine cellulose microfibril orientation more accurately. However, this approach posed a big challenge for data processing, since we had to obtain the Raman intensity of the cellulose peak at every polarization direction from each mapping position, perform ellipse fitting at all of the positions, and generate the corresponding graphs. It is not realistic to perform this procedure manually and the commercial Raman imaging software does not provide the functionality to do this analysis. To meet this challenge, we developed our own Matlab codes to realize automatic data processing.

In order to map out microfibril orientation at high spatial resolution, we made measurements at 42 positions at an interval of 0.5 μm in a leaf sheath section of the wild type rice plant (see Figure 4 a, b). Each of the polar plots in Figure 4c corresponds to a specific position marked in the bright field image. The director angle between cellulose microfibrils and

the longitudinal axis of the plant section at this position was determined by ellipse fitting (red line) of the measured data (blue circles). For the same positions, a quiver plot can be obtained as shown in Figure 4d where the arrow orientation indicates the director angle and the length of the arrow indicates the corresponding anisotropy magnitude. We found the director angle to be either 20° or 30° for the 42 positions measured. The anisotropy magnitude is quite uniformly distributed with an average of 0.24 and a standard deviation of 0.02. These results suggest that cellulose microfibrils are organized with a high degree of order within the leaf sheath cell walls.

We further utilized polarized Raman imaging in order to compare different tissues of the wild type rice plant. As illustrated in Figure 5, we measured the Raman signal for cellulose and lignin at 21 positions at an interval of 0.5 μm in a stem section and a leaf section of the wild type rice plant, respectively. Director angle and anisotropy magnitude of the stem and leaf sections are shown in the quiver plots in Figure 5. The detailed data for cellulose microfibril orientation are summarized in Table 1. The director angle was either 20° or 30° for the 21 positions measured in the stem section, while it was either 10° or 20° for the 21 positions measured in the leaf section with an exception (30°) at one position, which is slightly narrower than the stem section. We observed a higher value for the anisotropy magnitude in stem section (average = 0.22, standard deviation = 0.02) compared to the leaf section (average = 0.14, standard deviation = 0.02), indicating a higher degree of order of the cellulose microfibers in the stem section, with a cellulose microfibril orientation being very close to the value we obtained in the leaf sheath section. In addition to cellulose orientation, we also examined lignin orientation, and found that there was no preferred orientation of aromatic rings of lignin in the longitudinal plane of either

15

the stem section or the leaf section of the wild type rice plant, consistent with our previous observation in the wild type leaf sheath section (see Figure 2e).

The current work is a proof-of-concept study. The proposed approach can be applied to different plant species, different tissue and cell types. Also, changes of fiber orientation caused by different physical, chemical and biochemical treatments can be monitored for different industrial applications. To increase the speed of data acquisition, measurement could be performed at polarization direction from 0° to 90° instead of 0° to 360° given the data quality presented in this study.

CONCLUSIONS

In this study, we have demonstrated the use of polarized Raman microspectroscopy to measure the spatial distribution of cellulose microfibril orientation within cell walls of rice, which is a fundamental property determining mechanical strength of cell walls and was insufficiently studied in the past due to limitation of measurement techniques. We determined both the director angle - the angle between the cellulose microfibrils and the longitudinal axis of the cell wall, as well as the anisotropy magnitude - the degree of fiber organization. Utilizing this method, we were able to determine differences in cellulose microfibril orientation between wild type and mutant rice plants and between different tissues of a wild type rice plant. To the best of our knowledge, this is the first time that polarized Raman microspectroscopy or Raman imaging was used to determine the spatial distribution of cellulose microfibril orientation within cell walls of herbaceous plants and to compare cellulose microfibril orientation in cell walls between wild

type and mutant plants. This method can be readily extended to other plant species for both fundamental studies and applied (e.g. biofuel) applications.

ACKNOWLEDGMENT

This work conducted by the Joint BioEnergy Institute was supported by the Office of Science, Office of Biological and Environmental Research of the U.S. Department of Energy under contract no. DE-AC02-05CH11231. There are no potential sources of conflict of interest.

REFERENCES

Abe H, Ohtani J, Fukazawa K. 1991. FE-SEM observations on the microfibrillar orientation in the secondary wall of tracheids. IAWA Bulletin n.s. 12(4):431-438.

Agarwal U. 2006. Raman imaging to investigate ultrastructure and composition of plant cell walls: distribution of lignin and cellulose in black spruce wood (Picea mariana). Planta 224(5):1141-1153.

Agarwal UP, Atalla RH. 1986. In-situ Raman microprobe studies of plant cell walls: Macromolecular organization and compositional variability in the secondary wall of Picea mariana (Mill.) B.S.P. Planta 169(3):325-332.

Atalla RH, Agarwal UP. 1985. Raman Microprobe Evidence for Lignin Orientation in the Cell Walls of Native Woody Tissue. Science 227(4687):636-638.

Atalla RH, Agarwal UP. 1986. Recording Raman spectra from plant cell walls. Journal of Raman Spectroscopy 17(2):229-231.

17

Atalla RH, Whitmore RE, Heimbach CJ. 1980. Raman Spectral Evidence for Molecular Orientation in Native Cellulosic Fibers. Macromolecules 13(6):1717-1719.

Barnett JR, Bonham VA. 2004. Cellulose microfibril angle in the cell wall of wood fibres. Biological Reviews 79(2):461-472.

Booker RE, Sell J. 1998. The nanostructure of the cell wall of softwoods and its functions in a living tree. Holz als Roh- und Werkstoff 56(1):1-8.

Cao Y, Shen D, Lu Y, Huang Y. 2006. A Raman-scattering Study on the Net Orientation of Biomacromolecules in the Outer Epidermal Walls of Mature Wheat Stems (Triticum aestivum). Ann. Bot. 97(6):1091-1094.

Cave ID. 1997. Theory of X-ray measurement of microfibril angle in wood. Wood Science and Technology 31(3):143-152.

Dokken KM, Davis LC, Marinkovic NS. 2005. Use of Infrared Microspectroscopy in Plant Growth and Development. Appl. Spectrosc. Rev. 40(4):301 - 326.

Donaldson L. 2008. Microfibril angle: measurement, variation and relationships - a review. IAWA Journal 29(4):345-386.

Donaldson L, Frankland A. 2005. Ultrastructure of iodine treated wood. Holzforschung 58(3):219-225.

Donaldson L, Xu P. 2005. Microfibril orientation across the secondary cell wall of Radiata pine tracheids. Trees: Structure and Function 19(6):644-653.

Evans CL, Xie XS. 2008. Coherent Anti-Stokes Raman Scattering Microscopy: Chemical Imaging for Biology and Medicine. Annual Review of Analytical Chemistry 1(1):883-909.

Gierlinger N, Luss S, König C, Konnerth J, Eder M, Fratzl P. 2010. Cellulose microfibril orientation of Picea abies and its variability at the micron-level determined by Raman imaging. J. Exp. Bot. 61(2):587-595.

Gierlinger N, Schwanninger M. 2006. Chemical Imaging of Poplar Wood Cell Walls by Confocal Raman Microscopy. Plant Physiol. 140(4):1246-1254.

Goswami T, Saikia CN, Baruah RK, Sarma CM. 1996. Characterization of pulp obtained from Populus deltoides plants of different ages using IR, XRD and SEM. Bioresour. Technol. 57(2):209-214.

Huang C-L. 1995. Revealing Fibril Angle in Wood Sections By Ultrasonic Treatment. Wood and Fiber Science 27(1):49-54.

Kovur SK, Schenzel K, Diepenbrock W. 2008. Orientation Dependent FT Raman Microspectroscopy on Hemp Fibers. Macromolecular Symposia 265(1):205-210.

Lichtenegger H, Müller M, Paris O, Riekel C, Fratzl P. 1999. Imaging of the helical arrangement of cellulose fibrils in wood by synchrotron X-ray microdiffraction. Journal of Applied Crystallography 32(6):1127-1133.

Madakadze IC, Radiotis T, Li J, Goel K, Smith DL. 1999. Kraft pulping characteristics and pulp properties of warm season grasses. Bioresour. Technol. 69(1):75-85.

Palviainen J, Silvennoinen R, Rouvinen J. 2004. Analysis of microfibril angle of wood fibers using laser microscope polarimetry. Optical Engineering 43(1):186-191.

Peter GF, Benton DM, Bennett K. 2003. A simple, direct method for measurement of microfibril angle in single fibres using differential interference contrast microscopy. Journal of Pulp and Paper Science 29(8):274-280.

Schimleck L, Evans R, Ilic J. 2001a. Application of near infrared spectroscopy to a diverse range of species demosntrating wide density and stiffness variation. IAWA Journal 22(4):415-429.

Schimleck LR, Evans R. 2002. Estimation of microfibril angle of increment cores by near infrared spectroscopy. IAWA Journal 23(3):225-234.

Schimleck LR, Evans R, Ilic J. 2001b. Estimation of Eucalyptus delegatensis wood properties by near infrared spectroscopy. Canadian Journal of Forest Research 31(10):1671-1675.

Smith-Moritz AM, Chern M, Lao J, Sze-To WH, Heazlewood JL, Ronald PC, Vega-Sánchez ME. 2011. Combining multivariate analysis and monosaccharide composition modeling to identify plant cell wall variations by Fourier Transform Near Infrared spectroscopy. Plant Methods C7 - 26 7(1):1-13.

Sun L, Li C, Xue Z, Simmons BA, Singh S. 2013. Unveiling high-resolution, tissue specific dynamic changes in corn stover during ionic liquid pretreatment. RSC Advances 3(6):2017-2027.

Sun L, Simmons BA, Singh S. 2011. Understanding tissue specific compositions of bioenergy feedstocks through hyperspectral Raman imaging. Biotechnol. Bioeng. 108(2):286-295.

Tanaka K, Murata K, Yamazaki M, Onosato K, Miyao A, Hirochika H. 2003. Three Distinct Rice Cellulose Synthase Catalytic Subunit Genes Required for Cellulose Synthesis in the Secondary Wall. Plant Physiol. 133(1):73-83.

Varanasi P, Katsnelson J, Larson DM, Sharma R, Sharma MK, Vega-Sánchez ME, Zemla M, Loque D, Ronald PC, Simmons BA and others. 2012. Mechanical stress analysis as a

method to understand the impact of genetically engineered rice and arabidopsis plants. Industrial Biotechnology 8(4):238-244.

Vega-Sanchez ME, Verhertbruggen Y, Christensen U, Chen X, Sharma V, Varanasi P, Jobling SA, Talbot M, White RG, Joo M and others. 2012. Loss of Cellulose Synthase-Like F6 function affects mixed-linkage glucan deposition, cell wall mechanical properties and defense responses in vegetative tissues of rice. Plant Physiol.

Wiley JH, Atalla RH. 1987. Band assignments in the raman spectra of celluloses. Carbohydrate Research 160:113-129.

Ye C. 2006. Spectroscopic imaging ellipsometry: real-time measurement of single, intact wood pulp fibers. Appl. Opt. 45(36):9092-9104.

Zhang B, Zhou Y. 2011. Rice Brittleness Mutants: A Way to Open the 'Black Box' of Monocot Cell Wall BiosynthesisFree Access. Journal of Integrative Plant Biology 53(2):136-142.

Zhang M, Zhang B, Qian Q, Yu Y, Li R, Zhang J, Liu X, Zeng D, Li J, Zhou Y. 2010. Brittle Culm 12, a dual-targeting kinesin-4 protein, controls cell-cycle progression and wall properties in rice. The Plant Journal 63(2):312-328.

Zimmerley M, Younger R, Valenton T, Oertel DC, Ward JL, Potma EO. 2010. Molecular Orientation in Dry and Hydrated Cellulose Fibers: A Coherent Anti-Stokes Raman Scattering Microscopy Study. The Journal of Physical Chemistry B 114(31):10200-10208.

21

Table 1. Summary of director angle and anisotropy magnitude of the stem and leaf sections of the wild type rice plant.

Positions	Wild Type Rice Stem						Wild Type Rice Leaf					
Row: X	Director Angle*			Anisotropy Magnitude			Director Angle			Anisotropy Magnitude		
Column: Y	1	2	3	1	2	3	1	2	3	1	2	3
1	30	30	20	0.21	0.21	0.24	20	10	20	0.13	0.14	0.11
2	20	30	20	0.22	0.19	0.24	20	20	20	0.14	0.14	0.12
3	30	20	20	0.15	0.23	0.22	20	20	20	0.18	0.12	0.16
4	20	20	20	0.22	0.24	0.22	20	20	20	0.17	0.13	0.14
5	20	20	30	0.22	0.21	0.24	20	20	30	0.09	0.17	0.11
6	30	20	20	0.23	0.18	0.24	20	10	20	0.13	0.13	0.13
7	20	20	20	0.23	0.23	0.20	20	20	20	0.14	0.13	0.14
Average	20			0.22			20			0.14		
SD#	0			0.02			0			0.02		

* The resolution of director angle measurement was 10° in this work.

SD means standard deviation.

22

LIST OF FIGURES

Figure 1. Schematic of the experimental set-up. (a) Polarization direction of the incident laser is rotated 2θ when the half-wave plate is rotated θ. The step of θ is 5 degrees. The red arrow indicates the polarization direction of the laser beam. (b) The longitudinal section of the plant material is mounted on the stage of an inversed microscope. The red arrow indicates the polarization direction of the excitation laser.

Figure 2. Determination of cellulose and lignin orientation at a single position in a leaf sheath sample of wild type (RGT3584-WT) rice. (a) Raman spectra in the spectral range of 200-1700 cm^{-1}; (b) Raman spectra in the zoomed-in spectral range of 1017-1218 cm^{-1} after baseline correction in this range, where peaks at 1095 cm^{-1} and 1122 cm^{-1} are major cellulose peaks. (c) Determination of cellulose microfibril orientation using polar plot drawn from intensity data at 1095 cm^{-1}; (d) Determination of cellulose microfibril orientation using polar plot drawn from intensity data at 1122 cm^{-1}; (e) Determination of lignin orientation using polar plot drawn from intensity data at 1600 cm^{-1}. In the polar plots, the blue circles denote the measured data, the red lines are the results of ellipse fitting, and ρ is the anisotropy magnitudes determined by the lengths of the long and short axes of the fitted eclipses in (c)-(e).

Figure 3. Point measurements of leaf sheath samples of wild type (RGT3584-WT) and *brittle culm* (RGT3584-bc) mutant rice plants. (a) Bright field images of the wild type sample with six different positions marked for measurement; (b) Polar plots of Raman signals at 1095 cm^{-1} collected from these six different positions in the wild type sample, where ρ indicates the

23

corresponding anisotropy magnitude at these positions; (c) Bright field images of the *brittle culm* sample with six different positions marked for measurements; (d) Polar plots of Raman signals at 1095 cm^{-1} collected from these six different positions in the *brittle culm* sample, where ρ indicates the corresponding anisotropy magnitude at these positions.

Figure 4. Determination of cellulose microfibril orientation within leaf sheath section of wild type (RGT3584-WT) rice sample by Raman microspectroscopy. (a) Bright field image of the leaf sheath section with the marked area for measurement. (b) Blow-up image of the marked area. (c) Polar plots of Raman intensity at 1095 cm^{-1} obtained from individual positions of the leaf sheath section. (d) Quiver plot of distribution of cellulose microfibril orientation within the measured area. In the polar plots, the blue circles denote the measured data and the red lines are the results of ellipse fitting. In the quiver plot, the arrow direction indicates the director angle at the specific position in the image and the length of the arrow indicates the corresponding anisotropy magnitude.

Figure 5. Distribution of biopolymer orientation within the cell walls of (a) wild type (RGT3584-WT) rice stem and (b) rice leaf. Top: bright images of selected areas for imaging; Bottom left: Quiver plots of cellulose orientation; Bottom right: Quiver plots of lignin orientation. In the quiver plots, the arrow direction indicates the director angle at the specific position in the images and the length of the arrow indicates the corresponding anisotropy magnitude. Length of one arrow is labeled in the each of the quiver plots to show the scale. All quiver plots are generated in the same scale for easier comparison.

Figure 1

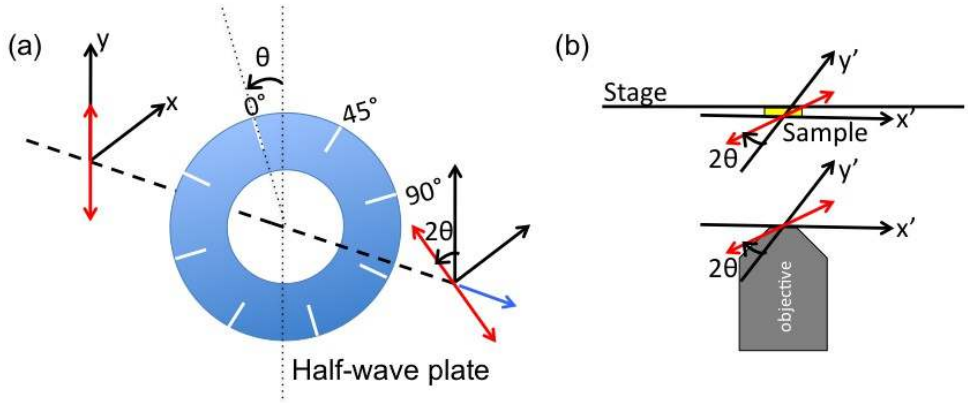
(a)
y
x
θ
0°
45°
90°
2θ
Half-wave plate
(b)
Stage
y'
x'
Sample
2θ
y'
x'
2θ
objective

25

Figure 2.

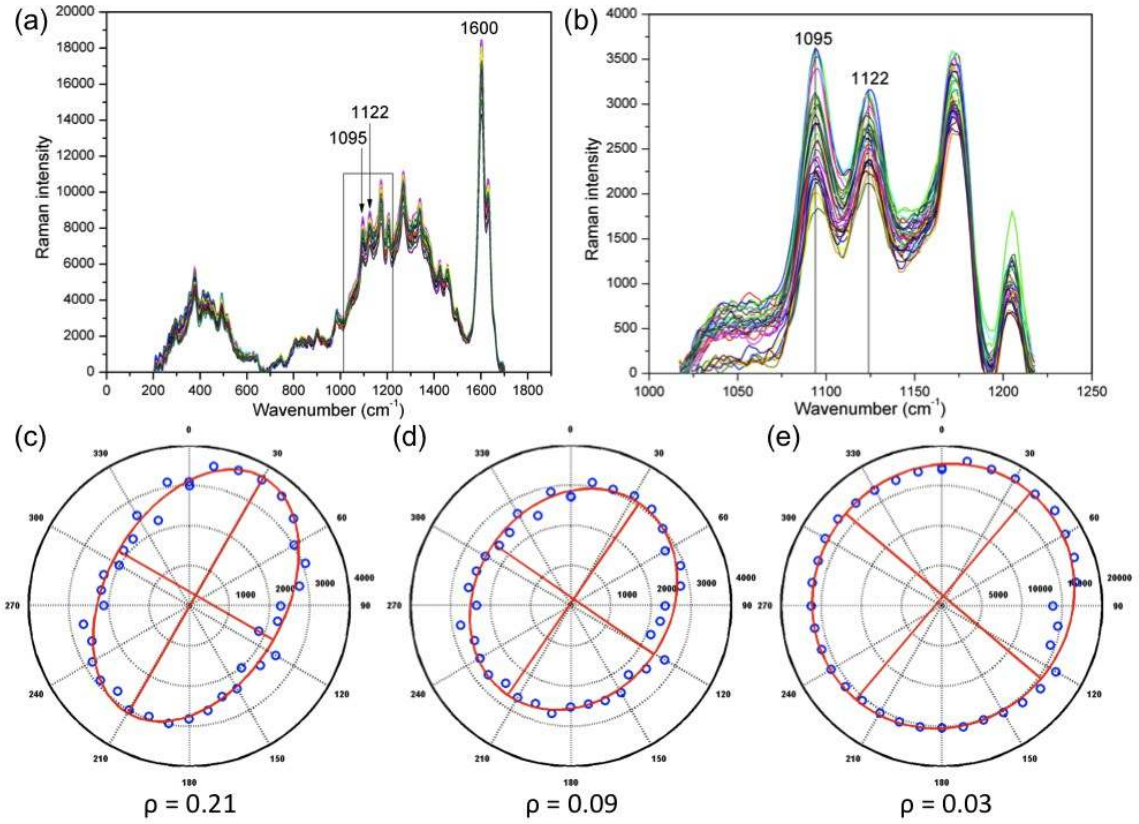
(a)
1600
1122
1095
Raman intensity
Wavenumber (cm-1)
(b)
1095
1122
Raman intensity
Wavenumber (cm-1)
(c)
ρ = 0.21
(d)
ρ = 0.09
(e)
ρ = 0.03

26

Figure 3

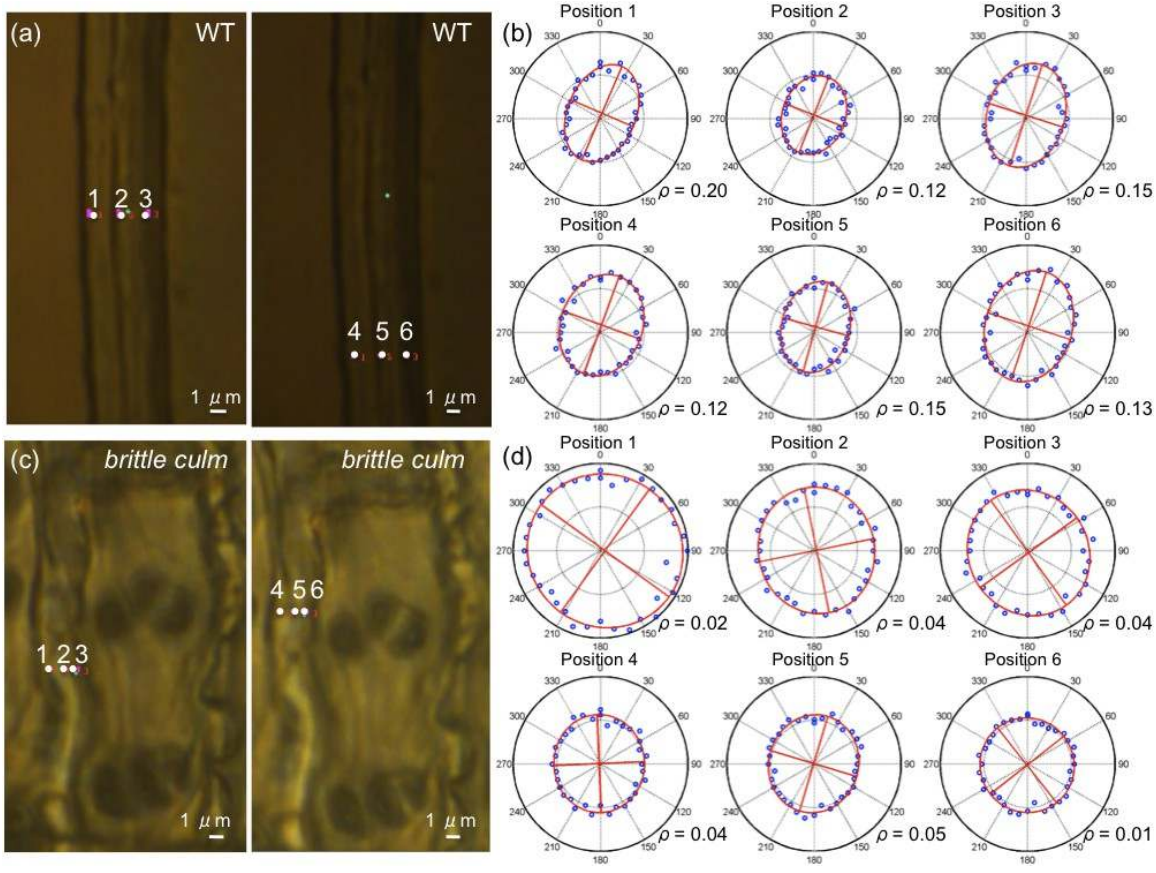
(a)
WT
1 2 3
1 μm
WT
4 5 6
1 μm
(b)
Position 1
ρ = 0.20
Position 2
ρ = 0.12
Position 3
ρ = 0.15
Position 4
ρ = 0.12
Position 5
ρ = 0.15
Position 6
ρ = 0.13
(c)
brittle culm
1 2 3
1 μm
brittle culm
4 5 6
1 μm
(d)
Position 1
ρ = 0.02
Position 2
ρ = 0.04
Position 3
ρ = 0.04
Position 4
ρ = 0.04
Position 5
ρ = 0.05
Position 6
ρ = 0.01

27

Figure 4

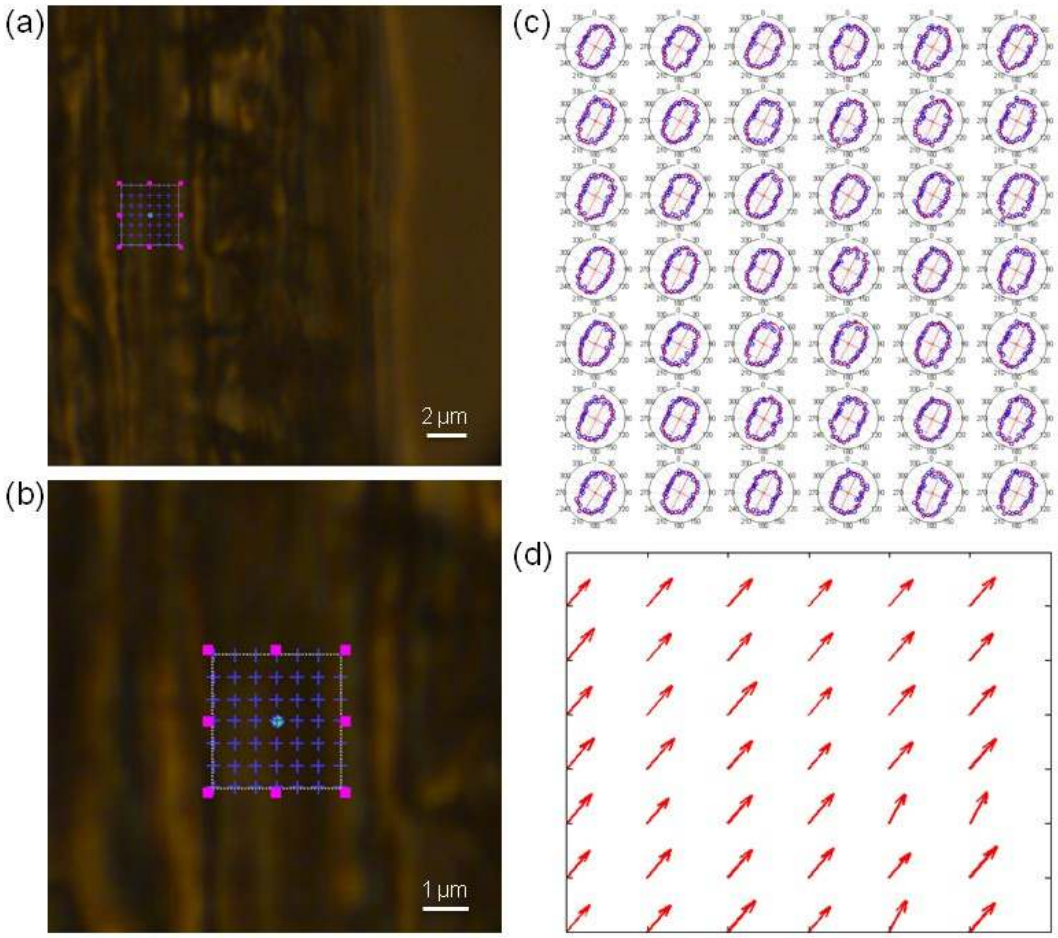

28

Figure 5

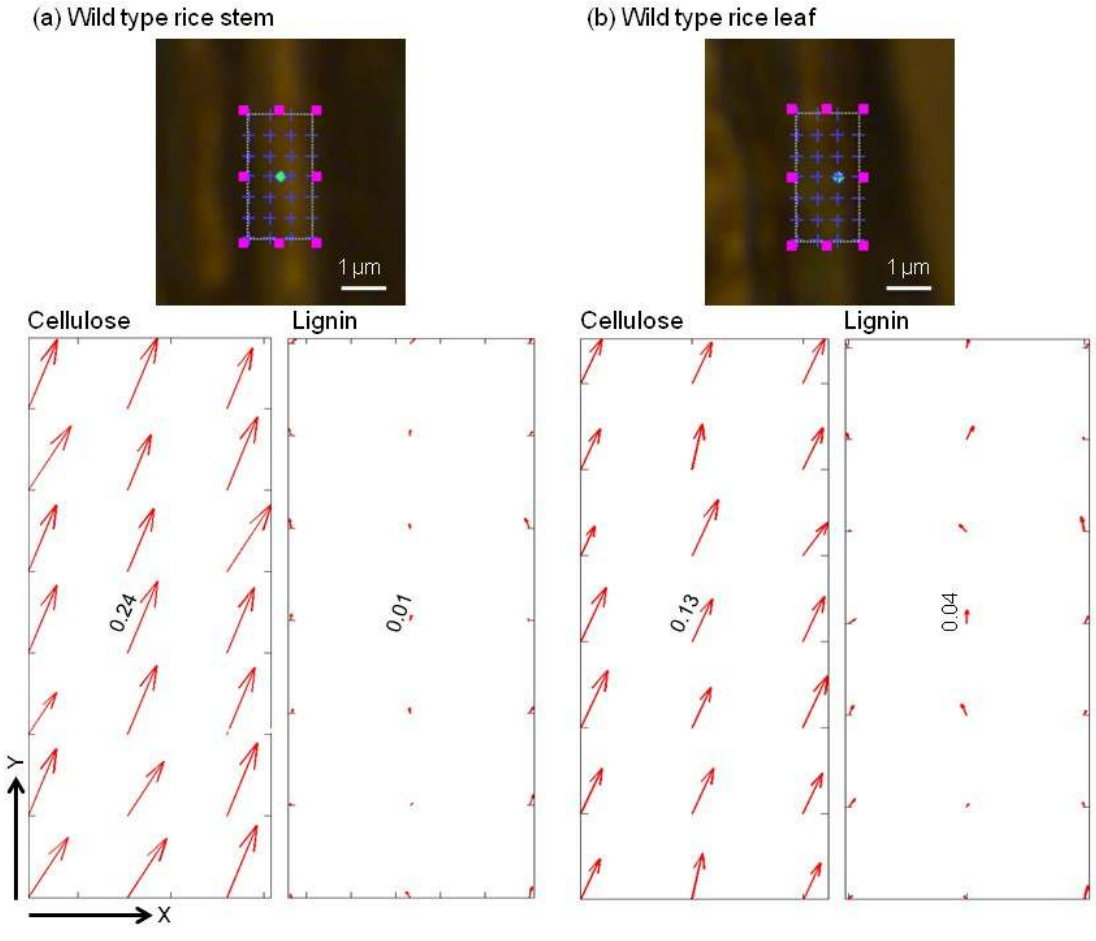
(a) Wild type rice stem
1 μm
Cellulose
Lignin
0.24
0.01
(b) Wild type rice leaf
1 μm
Cellulose
Lignin
0.13
0.04
Y
X

29

Table of Contents Graphic

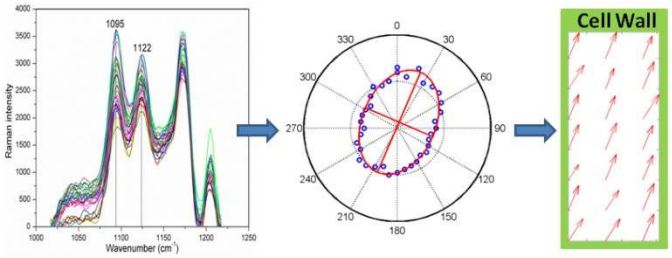

The authors developed a noninvasive polarized Raman microspectroscopic method to determine distribution of cellulose microfibril orientation within rice plant cell walls. Clear differences in cellulose microfibril orientation were observed between different tissues of the wild type rice plant as well as between the wild type and the *brittle culm* mutant, a mutant compromised in secondary cell wall deposition. This is the first time that polarized Raman microspectroscopy was used to determine supramolecular organization in cell walls for herbaceous plants.

30